IET Power Electronics

Special issue Call for Papers

Be Seen. Be Cited.
Submit your work to a new IET special issue

Connect with researchers and experts in your field and share knowledge.

Be part of the latest research trends, faster.

Read more

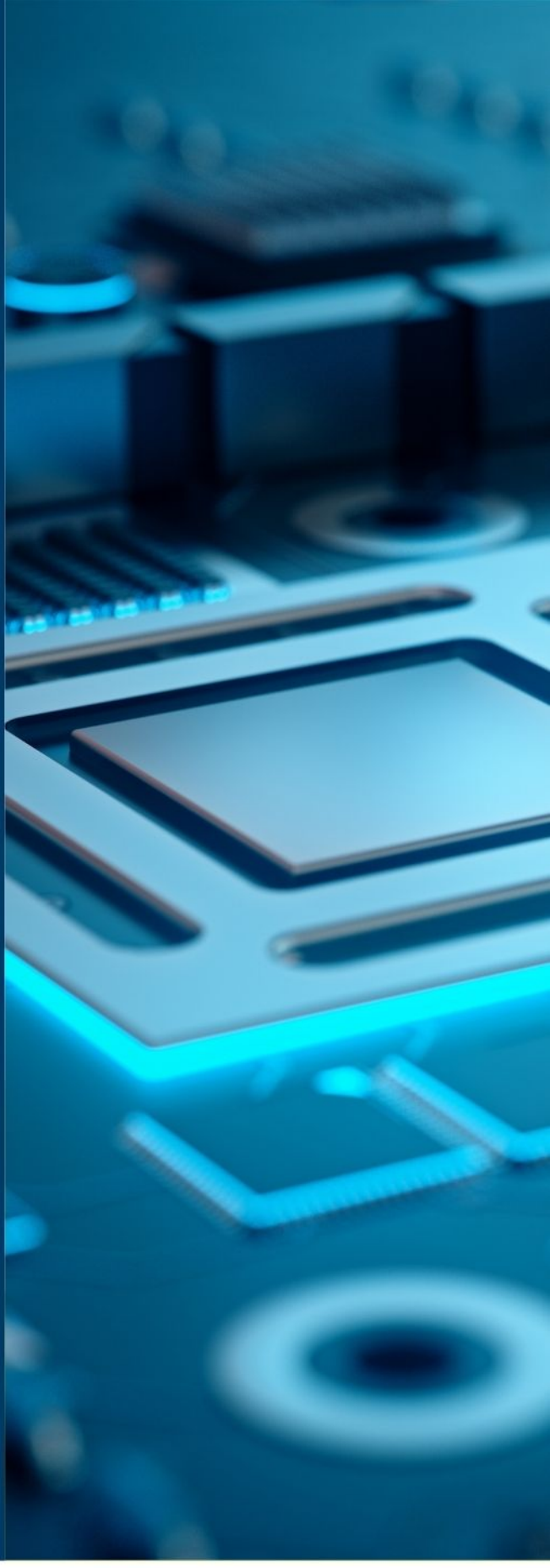

The Institution of Engineering and Technology

Received: 1 December 2022 | Revised: 11 May 2023 | Accepted: 16 May 2023

IET Power Electronics

DOI: 10.1049/pel2.12530

The Institution of Engineering and Technology WILEY

ORIGINAL RESEARCH

Low-ripple high-efficiency AC-DC rectifier with auxiliary compensator for hydrogen production

Li Zhang[1] | **Minxiao Han**[1] | **Weiqi Bao**[1] | **Yijiang Dong**[1] | **Yiwen Fan**[1] | **Haijun Liu**[2]

[1]School of Electrical and Electronic Engineering, North China Electric Power University, Beijing, People's Republic of China

[2]State Key Laboratory of Advanced Power Transmission Technology, State Grid Smart Grid Research Institute Co., Ltd., Beijing, People's Republic of China

Correspondence
Minxiao Han, School of Electrical and Electronic Engineering, North China Electric Power University, Beijing 100096, People's Republic of China.
Email: corresponding_han@163.com

Funding information
National Key Research and Development Plan of China, Grant/Award Number: 2020YFB1506800

Abstract

In hydrogen production, AC-DC rectifiers must provide a high current and low voltage to the production load. This paper focuses on the efficient performance and elimination of the output ripple in these AC-DC rectifiers. Unfortunately, efforts to reduce the current ripple often lead to lower efficiency, causing a contradiction. To address this issue, a low-ripple high-efficiency AC-DC rectifier with an auxiliary compensator is proposed in this paper. The proposed rectifier can maximise efficiency while eliminating the current ripple, including the switching ripple and low-frequency ripple. By incorporating a rectifier-chopper and a buck circuit with a series-connected capacitor, the auxiliary compensator, the solution provides an additional flow path for the current ripple at the rectifier output, successfully preventing the ripple from being output to the load. This paper offers a thorough exposition regarding the causative factors and sources of the switching and low-frequency ripple. Furthermore, a detailed explication of the operating principle of the proposed rectifier system is provided. The losses and costs associated with auxiliary compensators are then analysed for persuasive purposes. Finally, simulation and experimental results verify the feasibility and superiority of the proposed rectifier.

1 | INTRODUCTION

With the promotion of energy structure transformation in recent years, the global installed capacity of renewable energy sources such as wind turbines and photovoltaics continues to grow. However, the absorption problem of high proportion renewable energy has become increasingly prominent [1–3]. Energy storage technology can not only effectively alleviate the problem of renewable energy absorption but also improve the reliability of renewable energy supply [4]. As an efficient energy carrier, hydrogen is considered one of the vital energy storage forms for sustainable development in the future [5]. The combination of hydrogen and renewable energy has received increasing attention [6].

The typical hydrogen production system based on renewable energy is illustrated in Figure 1. The electrolyser is a hydrogen production device powered by a low voltage, high current DC source [7]. Therefore, there is a need for an AC-DC rectifier to connect the electrolyser to the AC bus. The AC-DC rectifier for electrolyser is usually concerned with several points such as power factor, efficiency, output ripple and cost [8]. The AC-DC rectifier is designed for high current and low voltage, so the output current ripple should be considered more. Ripple experiments have been implemented for alkaline and polymer electrolyte membrane electrolysers [9, 10]. The findings indicated that the current ripple output by rectifiers reduces the hydrogen production efficiency of the electrolyser. Moreover, the current ripple could damage the inside of the electrolyser and shorten its service life. Hence, it is imperative to minimise the current ripple in the rectifier.

There are four main types of AC-DC rectifiers currently used in electrolysers: diode-based rectifiers, thyristor-based rectifiers, rectifier-choppers and pulse width modulation (PWM) current-source rectifiers [11]. Diode-based rectifiers are widely used in industry, such as adjustable speed drives and dc power supplies. The main diode-based rectifier topologies are six-pulse bridge

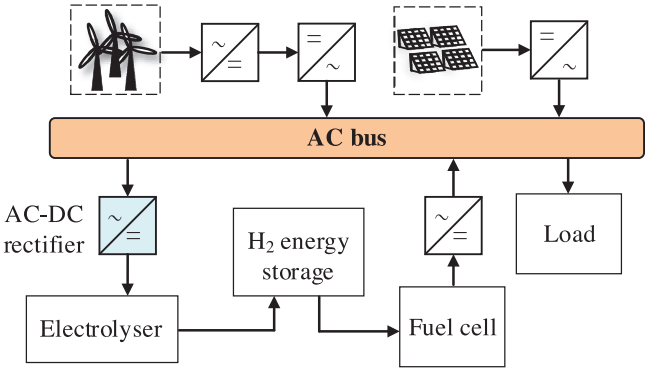

FIGURE 1 Typical hydrogen production system based on renewable energy.

rectifiers, multi-pulse bridge rectifiers and double-star rectifiers. Diode-based rectifiers feature low cost, high power factor and high efficiency, but the uncontrollability limits their application [12]. In contrast to diode-based rectifiers, thyristor-based rectifiers are controllable and facilitate control of the hydrogen flow rate and efficiency of the electrolyser. However, the reactive power of thyristor-based rectifiers is directly related to the firing angle. The increased firing angle greatly raises the input AC current harmonic content and reduces the power factor [8]. Therefore, thyristor-based rectifiers usually need both a large L-C passive filter network and an active filter to suppress input AC current harmonics and guarantee a power factor higher than 0.95 under all load conditions [8, 13]. In addition, adopting a multi-pulse rectifier topology can also effectively suppress input AC current harmonics. However, this leads to an increase in the complexity, cost and volume of rectifiers, as well as a reduction in the efficiency of the system [14]. Noteworthy diode-based rectifiers have a higher power factor, and typically, excellent current distortion suppression and power factor correction can be achieved simply by adding passive power filters without high additional costs and loss increases [14]. The rectifier-choppers usually consist of a diode-based rectifier and a DC-DC converter. The rectifier-chopper retains the advantages of diode-based rectifiers, while the cascaded DC-DC converter overcomes the uncontrollability of diode-based rectifiers [12]. The DC-DC converter adjusts the output current to control the hydrogen flow rate of the electrolyser featuring good controllability and fast dynamic response [15]. It has been proposed that PWM current-source rectifiers offer an alternative means of achieving excellent control over output current, high power factor, and fast dynamic response [16]. However, the insulated gate bipolar transistors (IGBTs) in such rectifiers are subject to high voltage and current stresses, which limit their applicability to high-power applications [8, 17]. It is reasonable to anticipate that with ongoing developments in IGBT technology, the losses they incur will eventually be substantially minimised. The silicon carbide (SiC) IGBT stands as an exemplar of this achievement [18]. Currently, SiC IGBT technology is still in its early stages and remains costly, thereby preventing its widespread adoption in the industrial sector.

The four types of AC-DC rectifiers mentioned above typically rely on filters to eliminate output ripple. However, bulky filters will be detrimental to the power losses, size and cost of the rectifiers [19, 20]. The rectifier-choppers and PWM current-source rectifiers can reduce ripple by increasing the switching frequency, but high switching frequency will significantly increase switching losses [5, 21]. The efficiency and output ripple of rectifiers present a contradictory relationship, often resulting in the need for a compromise. Therefore, the aim of this paper is to explore potential solutions to mitigate this conflict.

Considering various factors, including power factor, efficiency, output ripple, and cost, the rectifier-chopper emerges as the most balanced solution. The conventional rectifier-chopper for electrolyser applications consists of a diode bridge rectifier and a traditional buck converter. To increase output current and minimise output ripple, various combinations of rectifier-choppers have been proposed in recent years, such as diode bridge rectifier with an interleaved buck converter, diode bridge rectifier with a three-level interleaved converter, and diode bridge rectifier with a stacked interleaved buck converter [5, 8, 13, 22]. Nevertheless, these approaches have primarily emphasised eliminating switching ripple while not adequately considering the suppression of low-frequency ripple. This paper proposes a rectifier-chopper with an auxiliary compensator to enhance efficiency and minimise both the switching and low-frequency ripple. The application of the auxiliary compensator establishes a distinct path for these two types of ripples at the output of the rectifier-chopper, thereby averting any resulting ripple from reaching the load.

Section 2 explains the source of the switching and low-frequency ripple, and describes the operating principle of the proposed rectifier-chopper with the auxiliary compensator. In Section 3, the loss and cost associated with the auxiliary compensator are analysed for persuasive purposes. Besides, the feasibility and superiority of the proposed rectifier-chopper are verified by simulation and experimental results. Finally, conclusions are drawn in Section 4.

2 | THEORETICAL ANALYSIS

2.1 | Source of the output current ripple

This section explores the source of the rectifier-chopper output ripple. The traditional circuit structure of the rectifier-chopper can be described as the cascade of a diode-based bridge rectifier and a DC-DC converter. To meet the demand for high current output, DC-DC converters usually employ interleaved buck converters, as shown in Figure 2. D_i are diodes, $i = 1,2,\ldots,8$. S_{P1} and S_{P2} are switching tubes, L_{P1} and L_{P2} are filtering inductors with equal inductance, and C_d and C_P are filtering capacitors.

According to the fundamental theory of diode-based bridge rectifiers, output voltage fluctuations are influenced by loads, filter capacitors and other factors. The fluctuation range can be

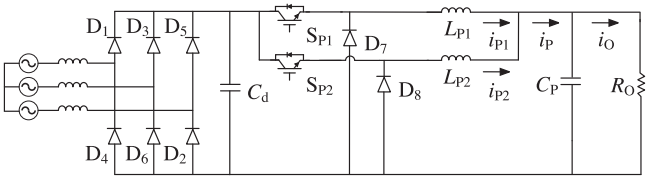

FIGURE 2 Traditional rectifier-chopper topology.

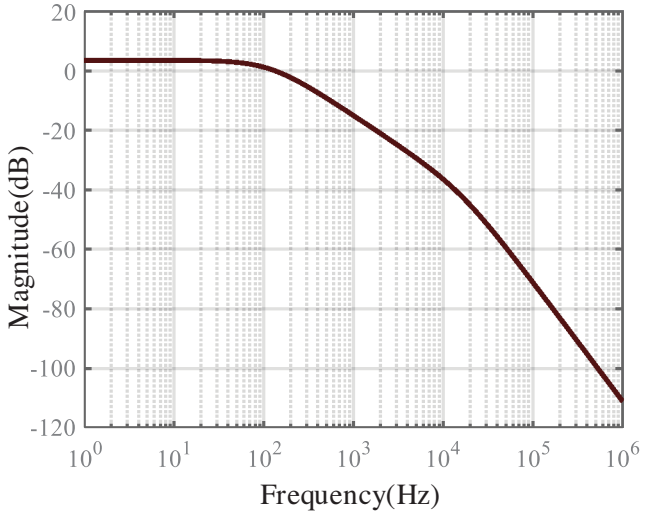

FIGURE 3 Frequency response diagram of the interleaved buck converter.

written as follows:

$$2.34U_2 < U_d < 2.45U_2, \tag{1}$$

where U_d is the voltage across capacitor C_d, U_2 is the RMS value of the phase voltage on the AC side.

The filter inductors and capacitors in interleaved buck converters form a low-pass filter, so the frequency response of the buck converter exhibits a low-pass characteristic. To clarify this characteristic, the transfer function of the buck converter is derived by state space averaging (SSA). SSA is a generic small-signal modelling method for converters. Assuming that the voltage harmonic Δv_d is applied to the voltage U_d, the converter output current ripple Δi_O can be determined by the following function:

$$G(s) = \frac{\Delta i_O(s)}{\Delta v_d(s)} = \frac{N(s)}{D(s)}$$

$$N(s) = D_P L_{P1} + D_p L_{P2}$$

$$D(s) = C_P L_{P1} L_{P2} R_O s^2 + L_{P1} L_{P2} s + L_{P1} R_O + L_{P2} R_O, \tag{2}$$

where D_P is the converter duty ratio, R_O is the load resistance.

The frequency response diagram can be drawn by substituting the converter parameters of the simulation model below into (2), as shown in Figure 3. When a six-pulse diode bridge rectifier is employed, the frequency of the voltage harmonic Δv_d is about

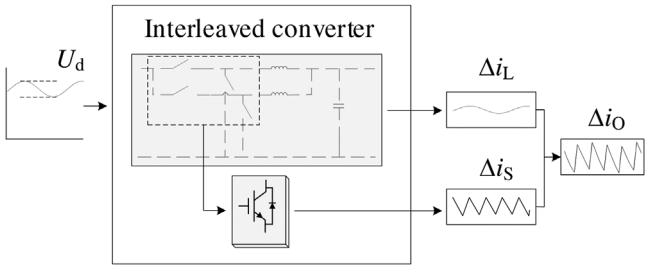

FIGURE 4 Interleaved converter ripple stacking diagram.

300Hz. According to Figure 3, the magnitude attenuation at 300Hz is only -5dB. This means that the buck converter rejects the input low-frequency voltage harmonics poorly, which will get through the buck converter and lead to the output ripple. In this paper, that output ripple is referred to as the low-frequency ripple.

In addition to low-frequency ripple, output ripple also includes switching ripple. The source of the switching ripple is the buck circuit, where switching operations cause inductors to charge and discharge repeatedly, resulting in fluctuations in output voltage and current. In high-current applications, output current ripple is of more concern. Assuming U_d is the ideal DC voltage, the fluctuation of current i_P in Figure 2 is the switching current ripple, and the peak-to-peak value of current i_P can be expressed as:

$$\Delta i_P = \frac{U_d(1 - ND_P)D_P}{f_P L_P}, \tag{3}$$

where D_P is the converter duty ratio, N is the number of parallel branches of the interleaved buck converter, f_P is the converter switching frequency, and L_P is the converter inductance.

The frequency of the switching ripple is equal to Nf_P, usually a few kHz. The switching ripple is, therefore, a medium-frequency fluctuation.

According to the above analysis, the output ripple of the converter is superimposed by switching ripple and low-frequency ripple, as shown in Figure 4. The former is generated by switching operations of the buck circuit, and the latter is generated by the fluctuation of voltage U_d. The converter will therefore output a current ripple superimposed by a low-frequency ripple Δi_L and a switching ripple Δi_S.

2.2 | Topology and control strategy of the proposed AC-DC rectifier

The proposed AC-DC rectifier is a rectifier-chopper with an auxiliary compensator. The auxiliary compensator is a buck circuit with a capacitor connected in series, as shown in Figure 5. The series capacitor C_b allows only AC power to pass through the auxiliary compensator. Therefore, it can be regarded that the auxiliary compensator provides a flow path for the output current ripple. The buck circuit in the auxiliary compensator employs the switching tube S_{C2} instead of the freewheeling

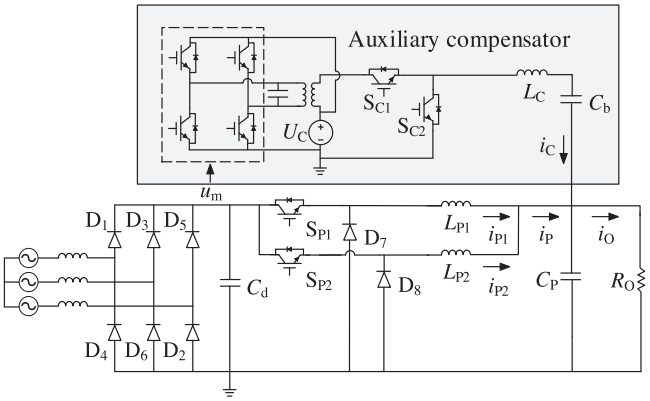

FIGURE 5 Rectifier-chopper with the auxiliary compensator.

TABLE 1 Relationship between each PWM control signal.

	S_{P1}	S_{P2}	S_{C1}	S_{C2}
Switching frequency	1	1	N	N
Duty ratio	D_P	D_P	D_C	1-D_C
Phase angle	0	$-\frac{1}{N}$	$\frac{D_C}{N}$	0

diode of the conventional buck circuit. In addition, there is a single-phase inverter circuit and a single-phase transformer, which form an isolated AC power supply. The single-phase inverter circuit derives its power from the DC supply U_C, and the modulating signal u_m generates from the current i_P. The secondary side of the single-phase transformer is connected in series with the DC supply U_C.

The control strategy of rectifier-choppers is mainly applied in DC-DC converters since diode-based rectifiers are not controllable. The DC-DC converter in this paper employs the interleaved buck converter. The switching tubes S_{P1} and S_{P2} in the interleaved buck converter are controllable. In addition, specific controls can be applied to the single-phase inverter circuit and the switching tubes S_{C1} and S_{C2} in the auxiliary compensator. The task of the auxiliary compensator is to eliminate the low-frequency ripple Δi_L and the switching ripple Δi_S output by the rectifier-chopper. The control strategy can be divided into two parts, for low-frequency ripple and switching ripple cancellation separately.

Firstly, the control strategy is introduced that can eliminate switching ripples. That control strategy is applied to the switching tubes S_{P1}, S_{P2}, S_{C1} and S_{C2}, which are controlled through PWM signals. Table 1 shows the relationship between each PWM control signal determined by duty ratio, frequency, and phase angle. The frequency and phase angle of the PWM control signals are expressed using the per-unit value, with the PWM signal of S_{P1} as the reference signal for the normalisation. The specified frequency, duty ratio and phase angle of the PWM control signals are adjusted through the carrier wave and modulating signals. N is the number of parallel branches of the interleaved buck converter, for example, $N = 2$ in a two-phase interleaved buck converter. Moreover, compared

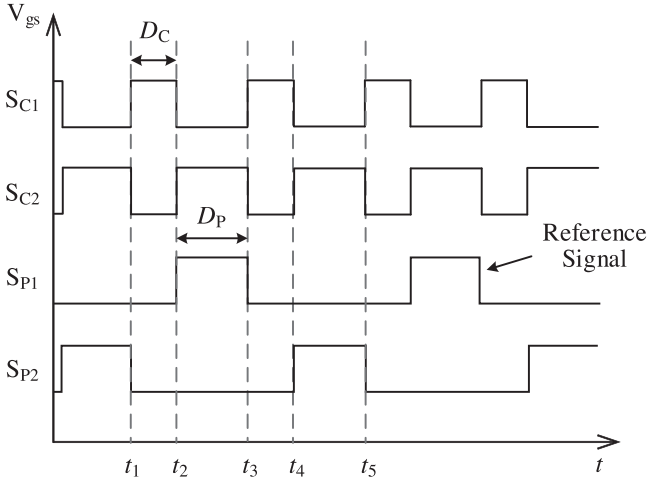

FIGURE 6 PWM signals for each buck circuit when $D_P = 0.3$.

to the reference signal, the PWM signal of S_{P2} has a phase lag of $1/N$, and the PWM signal of S_{C1} has a phase advance of D_C/N. The PWM signals of S_{C1} and S_{C2} in the auxiliary compensator are complementary. The same duty ratio D_P and switching frequency f_P are adopted by the PWM signals of both S_{P1} and S_{P2}. The switching frequency f_C of S_{C1} and S_{C2} is N times that of f_P. Their duty ratio D_C is calculated as follows:

$$D_C = \lceil D_P \cdot N \rceil - D_P \cdot N, \tag{4}$$

where $\lceil\rceil$ is meant to be rounded upward.

In order to better explain the relationship between each PWM signal, a specific case is given where $N = 2$, $D_P = 0.3$, as shown in Figure 6.

The difference in duty ratio between the auxiliary compensator and the interleaved converter results in a difference in the output voltage. Hence, a significant function of C_b is to achieve voltage dividing. The mathematical relations are obtained:

$$\begin{cases} U_O = U_d \cdot D_P \\ U_O + U_{Cb} = U_C \cdot D_C \end{cases}, \tag{5}$$

where U_{Cb} is the voltage across capacitor C_b, U_O is the output voltage.

The above control strategy can eliminate the switching ripple, and the next step is to consider how to reduce the low-frequency ripple. According to the analysis results in the previous section, the low-frequency ripple originates from the input voltage U_d of the interleaved buck circuit. Therefore, an AC fluctuation with a specific frequency, amplitude and phase can be superimposed on the DC supply of the auxiliary compensator. In this way, the auxiliary compensator will output an alternating current that is complementary to the low-frequency ripple. Their superposition can eliminate the low-frequency ripple.

The AC fluctuation superimposed on the DC supply of the auxiliary compensator is implemented using the single-phase inverter and the single-phase transformer. Both the inverter

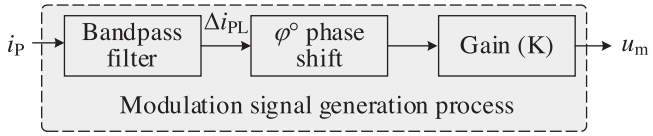

FIGURE 7 Modulation signals of the single-phase inverter.

and the transformer together form a controlled AC power supply whose frequency, amplitude and phase are consistent with modulation signals, as shown in Figure 7.

The modulation signal u_m is determined by the current i_P. The function of the band-pass filter will filter out the DC component and the switching ripple component of the current i_P. The output component Δi_{PL} of the band-pass filter has nearly the same amplitude and frequency as the low-frequency ripple Δi_L. Also note that their phase angle can be the same, as the band-pass filter can be designed to have a phase lag of 0 degrees at the frequency of the low-frequency ripple. Next, the phase of Δi_{PL} is delayed by φ^o and the phase-shifted Δi_{PL} is multiplied by the gain K to obtain the modulation signal u_m. The modulation signal u_m is compared with the carrier signal to obtain the inverter PWM control signal, which makes the secondary side of the transformer output the same AC voltage as the modulation signal u_m. The selection of parameters φ and K is related to the transfer function of the auxiliary compensator and can be written as follows:

$$\begin{cases} K = \dfrac{1}{H_C(\omega)} \\ \varphi = 180 - \varphi_C(\omega) \end{cases}, \tag{6}$$

where $H_C(\omega)$ is the amplitude-frequency response function of the auxiliary compensator, and $\varphi_C(\omega)$ is the phase-frequency response function.

2.3 | Analysis of the output current ripple

The output current ripple is related to the converter parameters and the control strategy. This paper assumes that each buck circuit of the interleaved buck converter operates in continuous conduction mode to avoid current loops between the parallel branches and the extra losses caused by the loops. Therefore, the switching frequency and inductance values can be calculated by:

$$L > L_B = \frac{U_d D_P^{\,2}}{2 f_P I_{max}} \cdot \frac{U_d - U_O}{U_O}, \tag{7}$$

where L_B is the boundary inductance, I_{max} is the maximum current of the buck circuit.

The existence of the capacitor C_b allows only AC power to flow through the auxiliary compensator. The capacitor C_b in the auxiliary compensator directly affects the switching ripple suppression effect of the converter. C_b must be reasonable so that the voltage fluctuation Δv_{Cb} across it varies very little during a switching cycle. Δv_{Cb} can be calculated by:

$$\Delta v_{Cb} = \frac{\Delta I_{Cb} \Delta t}{8 C_b}, \tag{8}$$

where ΔI_{Cb} is the current peak-to-peak value of the auxiliary compensator, C_b is the capacitance value, and Δt is the charge-discharge cycle.

Once the converter parameters have been selected, the output current ripple is analysed in conjunction with the control strategy. The output ripple of the converter is superimposed by switching ripple and low-frequency ripple. switching ripple and low-frequency ripple will be described separately for clarity of analysis.

Firstly, the output switching ripple is analysed. Assuming U_d is the ideal DC voltage, the fluctuation of current i_P is the switching current ripple. In this case, the current i_P contains no low-frequency ripple such that the output component Δi_{PL} of the bandpass filter is 0. Therefore, the inverter in the auxiliary compensator does not work, and the output voltage amplitude on the secondary side of the transformer is 0. As a result, the topology of the proposed rectifier-chopper can be simplified, as shown in Figure 8. The ripple formulae of the rectifier-chopper with duty ratio $D_P = 0.3$ is derived as an example, while the rest of the duty ratio is in the same derivation method. According to Figure 8, there are four operating stages in a cycle.

Stage 1 [t_1,t_2]: S_{C1} is turned on, S_{C2}, S_{P1} and S_{P2} are turned off. The inductor L_C is charged during this interval, and the inductors L_{P1} and L_{P2} are discharged. Applying Kirchhoff's voltage law, equations are obtained as follows:

$$\begin{cases} U_C - U_O - U_{Cb} - \Delta v_{Cb} = L_C \dfrac{di_C}{dt} = L_C \dfrac{\Delta i_C}{\Delta t} \\ -U_O = L_{P1} \dfrac{di_{P1}}{dt} = L_{P1} \dfrac{\Delta i_{P1}}{\Delta t} \\ -U_O = L_{P2} \dfrac{di_{P2}}{dt} = L_{P2} \dfrac{\Delta i_{P2}}{\Delta t} \\ U_O + U_{Cb} = D_C U_C \end{cases}, \tag{9}$$

where Δv_{Cb} is smaller by 1 to 2 orders of magnitude than U_{Cb}, so Δv_{Cb} can be ignored in the derivation of the formula. Δt can be expressed as:

$$\Delta t = \frac{1}{2}(1 - 2D_P) T_P = \frac{(1 - 2D_P)}{2 f_P}, \tag{10}$$

where T_P is the switching period of the converter. According to (4) (5) (9) (10), the current switching ripple through each branch is obtained:

$$\begin{cases} \Delta i_C = \dfrac{U_C (1 - 2D_P) D_P}{f_P L_C} \\ \Delta i_{P1} = -\dfrac{U_d (1 - 2D_P) D_P}{2 f_P L_{P1}} \\ \Delta i_{P2} = -\dfrac{U_d (1 - 2D_P) D_P}{2 f_P L_{P2}} \end{cases}. \tag{11}$$

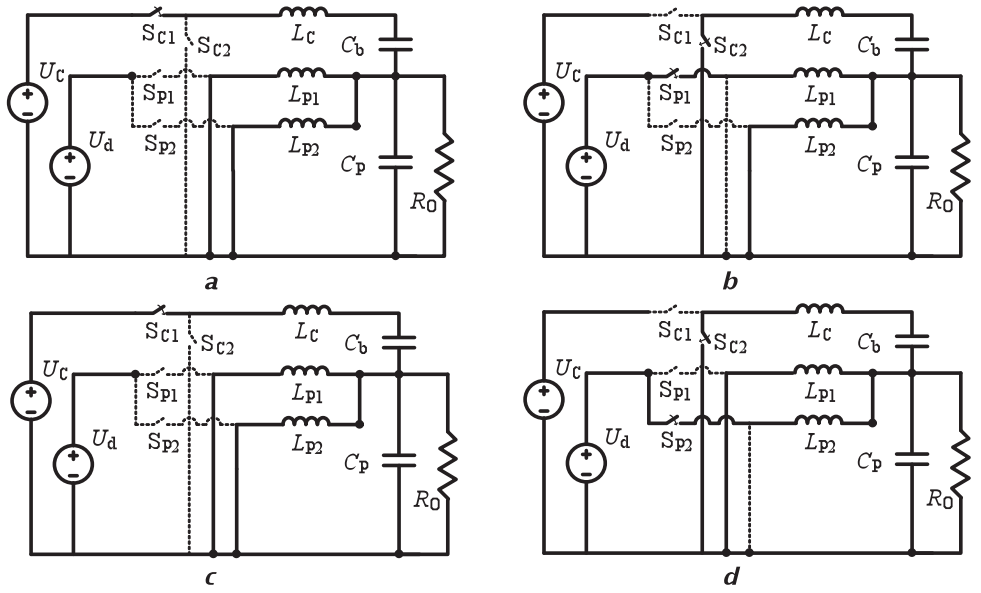

FIGURE 8 Operating stages of the simplified rectifier-chopper with the auxiliary compensator in a cycle. (a) Stage 1, (b) stage 2, (c) stage 3, (d) stage 4.

Assuming $U_C/L_C = U_d/L_{P1} = U_d/L_{P2}$, according to (11), the total output switching current ripple is obtained:

$$\Delta i_O = \Delta i_C + \Delta i_{P1} + \Delta i_{P2} = 0. \tag{12}$$

This stage ends when S_{C1} turns off at t_2.

Stage 2 [t_2,t_3]: S_{C2} and S_{P1} are turned on, S_{C1} and S_{P2} are turned off. The inductor L_{P1} is charged during this interval, and the inductors L_C and L_{P2} are discharged. Applying Kirchhoff's voltage law, equations are obtained as follows:

$$\begin{cases} -U_O - U_{Cb} + \Delta v_{Cb} = L_C \dfrac{di_C}{dt} = L_C \dfrac{\Delta i_C}{\Delta t} \\ U_d - U_O = L_{P1} \dfrac{di_{P1}}{dt} = L_{P1} \dfrac{\Delta i_{P1}}{\Delta t} \\ -U_O = L_{P2} \dfrac{di_{P2}}{dt} = L_{P2} \dfrac{\Delta i_{P2}}{\Delta t} \\ U_O + U_{Cb} = D_C U_C \end{cases}, \tag{13}$$

where the variable Δv_{Cb} is ignored, and $\Delta t = D_P T_P$. According to (4) (5) (13), the switching current ripple through each branch is obtained:

$$\begin{cases} \Delta i_C = -\dfrac{U_C(1-2D_P)D_P}{f_P L_C} \\ \Delta i_{P1} = \dfrac{U_d(1-D_P)D_P}{f_P L_{P1}} \\ \Delta i_{P2} = -\dfrac{U_d D_P^2}{f_P L_{P2}} \end{cases}. \tag{14}$$

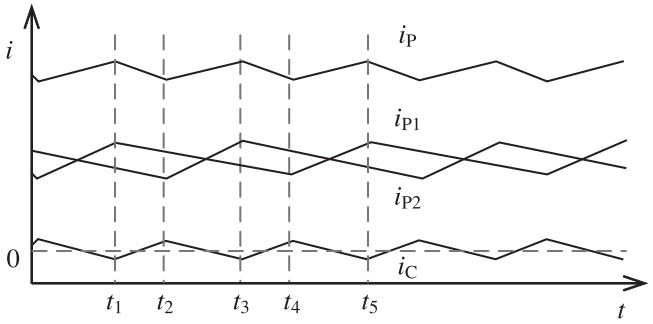

FIGURE 9 Branch currents of the rectifier-chopper at $D_P = 0.3$.

Assuming $U_C/L_C = U_d/L_{P1} = U_d/L_{P2}$, according to (14), the total output switching current ripple is obtained:

$$\Delta i_O = \Delta i_C + \Delta i_{P1} + \Delta i_{P2} = 0. \tag{15}$$

This stage ends when S_{C1} turns on at t_3.

Stage 3 [t_3,t_4] is the same as *Stage 1*, where the inductor L_C is charged, and the inductors L_{P1} and L_{P2} are discharged. Hence the current ripple formulae are the same for both stages. *Stage 4 [t_4,t_5]* is analogous to *Stage 2*. The interleaved converter's inductor in one branch is charged while another inductor and L_C are discharged. Therefore, the current ripple equation is similar. The current waveforms of the four stages are given in Figure 9. It can be observed that the alternating current i_C of the auxiliary compensator and the output current i_P of the two-phase interleaved converter are complementary.

Secondly, the output low-frequency ripple is analysed. In this case, fluctuations in the input voltage U_d of the interleaved buck circuit will be taken into account. According to the previous theoretical analysis, the interleaved buck circuit is equivalent

to a low-pass filter. Input voltage fluctuations passing through the filter will generate the output low-frequency current ripple. Assuming that the low-frequency ripple $\Delta i_L = I\sin(\omega t)$, and therefore the output component Δi_{PL} of the bandpass filter in the inverter control is equal to Δi_L. Then shift Δi_{PL} by $\varphi°$ and multiplies it by the gain K. The modulation signal and the secondary voltage of the transformer u_m is derived as:

$$u_m = KI\sin(\omega t - \varphi). \tag{16}$$

From Equations (6) and (16), the low-frequency output current Δi_{CL} of the auxiliary compensator is obtained as:

$$\begin{aligned}\Delta i_{CL} &= KH_C(\omega) I\sin(\omega t - \varphi - \varphi_C(\omega)).\\ &= I\sin\left(\omega t - 180°\right)\end{aligned} \tag{17}$$

With the superposition of the auxiliary compensator output current Δi_{CL} and the interleaved converter output current Δi_L, the final low-frequency output current Δi_{OL} can be expressed as:

$$\Delta i_{OL} = \Delta i_L + \Delta i_{CL} = I\sin(\omega t) + I\sin(\omega t - 180) = 0. \tag{18}$$

2.4 | Loss analysis of rectifier-choppers

In the rectifier-chopper, the losses come mainly from switching tubes, diodes, and inductors. The losses in switching tubes consist of switching losses and conduction losses. The conduction loss can be calculated by:

$$P_{SC} = \frac{1}{T_S}\int_0^{T_S} U_{CE}(t) i_{CE}(t) D dt, \tag{19}$$

where T_S is the cycle time, $U_{CE}(t)$ is the forward voltage drop, $i_{CE}(t)$ is the collector-emitter current, and D is the duty ratio.

The relationship curve between U_{CE} and i_{CE} is non-linear. To simplify the calculation, the curve can be linearised and U_{CE} can be written as:

$$U_{CE}(t) = U_{CE0} + r_{CE} i_{CE}(t), \tag{20}$$

where U_{CE0} is the threshold voltage and r_{CE} is the equivalent resistance.

In general, the current and voltage curves during the turn-off and turn-on processes are approximated as straight lines for simple calculations. The switching loss of switching tubes can be calculated by:

$$P_{SS} = \frac{U_S I_M}{k} f_S (t_{on} + t_{off}), \tag{21}$$

where U_S is the off-state voltage, I_M is the maximum transient current, k is the load factor, f_S is the switching frequency, t_{on} is the turn-on time, t_{off} is the turn-off time. Turn-on time t_{on} and turn-off time t_{off} are influenced by the semiconductor material, voltage and temperature of switching tubes.

Diode losses include conduction losses and switching losses. The conduction loss can be calculated by:

$$P_{DC} = \frac{1}{T_D}\int_0^{T_{Don}} U_F(t) i_F(t) dt, \tag{22}$$

where T_D is the cycle time, T_{Don} is the turn-on time in a cycle, $U_F(t)$ is the forward voltage drop, and $i_F(t)$ is the forward current.

Switching losses are further divided into turn-on losses and turn-off losses. Since the turn-on time is very short, the turn-on loss is so small compared to the turn-off loss that it can be ignored. The turn-off loss can be calculated by:

$$P_{DS} = \frac{1}{2} U_{rf} I_{rf} t_f f_D, \tag{23}$$

where U_{rf} is the maximum transient voltage, I_{rf} is the maximum transient current, t_f is the reverse recovery time, f_D is the switching frequency of diodes.

The losses in inductors consist of coil losses and core losses. Since the inductors in rectifier-choppers are used for DC side filtering, the core loss is insignificant. This paper therefore focuses on the coil loss, which is mainly determined by the coil DC resistance. The coil loss can be calculated by:

$$P_L = I_{avg}^2 R_{dc}, \tag{24}$$

where I_{avg} is the average current and R_{dc} is the coil DC resistance.

Based on the output ripple analysis above, the auxiliary compensator can actively eliminate rectifier chopper output ripple without the need for high switching frequency and large filter inductor. As the switching frequency and inductor are reduced, the switching loss of the switching tubes and diodes will be reduced exponentially, as will the inductor loss.

3 | SIMULATION AND EXPERIMENTAL RESULTS

3.1 | Simulation validation

In this section, simulation models for the rectifier-choppers are built with the PSIM simulation Software. Firstly, the output current ripple of the proposed rectifier-chopper with the auxiliary compensator is simulated. To protrude the ripple cancellation effect of the auxiliary compensator, the output filter of the rectifier-chopper employs low capacitance C_P. The detailed parameters are shown in Table 2.

The switching frequency and filter inductance of the interleaved converter are determined by (7). Note that according

TABLE 2 Parameters of the simulation model.

Parameter	Value
Rectifier filter capacitor (C_d)	1 mF
Auxiliary DC power supply (U_C)	30 V
Auxiliary compensator inductor (L_C)	162 μH
Auxiliary compensator capacitor (C_b)	200 μF
Interleaved converter filter inductors (L_{P1}, L_{P2})	540 μH
Output filter capacitor (C_P)	50 μF
Output current (i_O)	100 A
Output voltage (V_O)	20 V
Interleaved converter switching frequency (f_P)	2 kHz
Auxiliary compensator switching frequency (f_C)	4 kHz

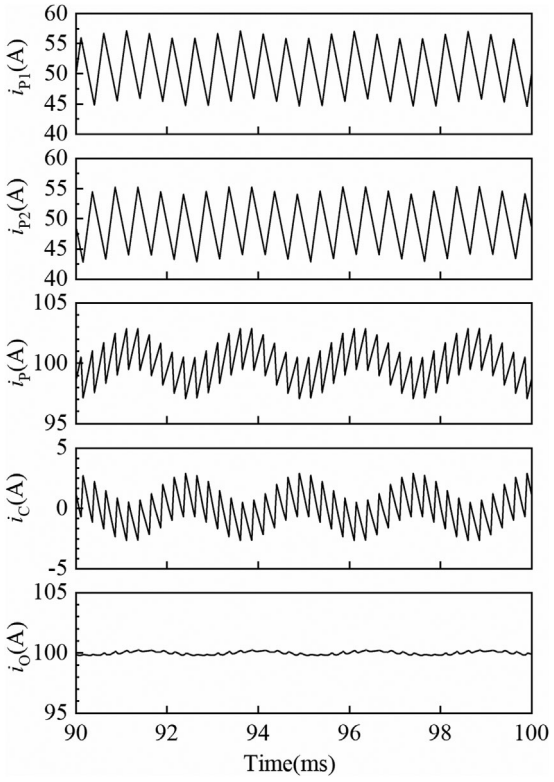

FIGURE 10 Current waveforms of the rectifier-chopper with the auxiliary compensator.

to the equation, this switching frequency and filter inductance can actually be reduced further, and it is also possible to reduce the filter inductance by increasing the switching frequency. As a result, their parameters can be adjusted to suit the actual situation. The rectifier-chopper in the simulation is set to a low-voltage high-current output to meet the supply requirements of the hydrogen production load. In this case, the output current is usually several times the output voltage and therefore current ripple should receive more attention.

The current waveforms of the rectifier-chopper with the auxiliary compensator are shown in Figure 10. The i_{P1} and i_{P2} are the currents in the two parallel branches of the interleaved converter. Both i_{P1} and i_{P2} consist of a low-frequency ripple and a medium-frequency switching ripple. The frequency of the low-frequency ripple is 300Hz, the same as the output voltage U_d of the rectifier, which implicitly indicates that the low-frequency ripple originates from the input voltage fluctuation of the interleaved converter. The frequency of the medium-frequency switching ripple is 2kHz. Next, i_{P1} and i_{P2} are superimposed to form the current i_P, which is the output current without the effect of the auxiliary compensator. The ripple of the current i_P can be observed to be around 6 A. The traditional method of eliminating this ripple is to increase the filter capacitance, inductance and switching frequency. However, the auxiliary compensator proposed in this paper allows the output ripple to be eliminated without using traditional methods. The current i_C in the auxiliary compensator branch is an AC component, which is complementary to the waveform of the output current ripple. Therefore, it can be considered that the auxiliary compensator provides a flow path for the output AC ripple so that this ripple is no longer output to the load side. With the auxiliary compensator, the output current ripple of the rectifier chopper is only 0.6 A. Compared with uncompensated current i_P, the ripple of the compensated output current i_O decreases by about ten times.

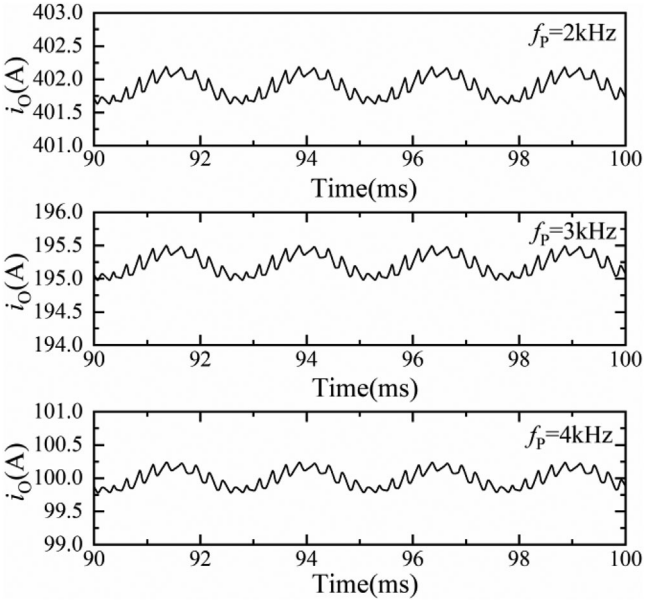

FIGURE 11 Output ripple at different output currents and switching frequencies.

In order to demonstrate the effectiveness of the proposed auxiliary compensator, several sets of tests were carried out at different output currents and switching frequencies. There are three groups of simulations, with output current and switching frequency corresponding to 100A/4kHz, 200A/3kHz, and 400A/2kHz, respectively. According to the simulation results in Figure 11, although the change in output current and switching frequency, the output current ripple stays around 0.6A with a maximum ripple coefficient of 0.3%. It is conducted that The auxiliary compensator is capable of eliminating the output

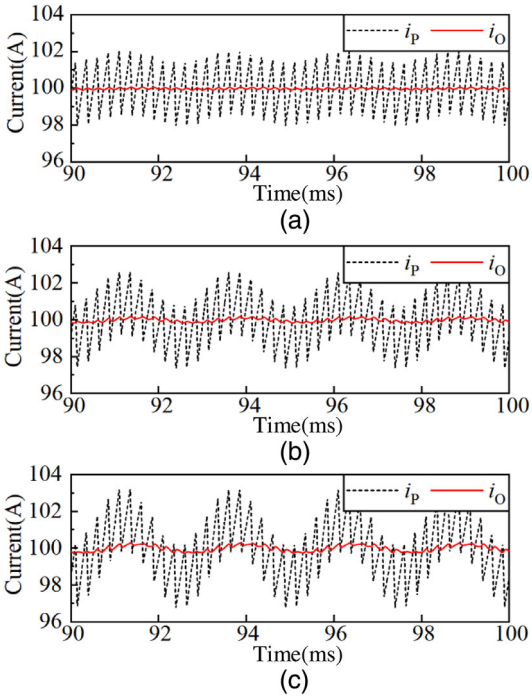

FIGURE 12 Comparison of output ripple using different rectifier output capacitors. (a) C_d=2 mF, (b) C_d=1.5 mF, (c) C_d=1 mF.

ripple of the rectifier chopper at different output currents and switching frequencies.

When the rectifier output filter capacitor C_d changes, the voltage fluctuation across the capacitor C_d varies accordingly, which will affect the output ripple of the rectifier-chopper. There are three sets of simulations, with the capacitances corresponding to 1mF, 1.5mF and 2mF. In Figure 12, i_P is the output ripple of the rectifier-chopper without the auxiliary compensator, and i_O is the output ripple of the rectifier-chopper with the auxiliary compensator. The comparison of simulation results indicates that the output ripple can be reduced about ten times with the effect of the auxiliary compensator. Faced with different voltage fluctuations across the capacitor C_d, the maximum output ripple of the rectifier-chopper with the auxiliary compensator is 0.6A, and the ripple coefficient is up to 0.3% among the three sets of simulations.

3.2 | Experimental verification

In order to verify the validity of the proposed rectifier-chopper with the auxiliary compensator, a 120W experimental prototype is implemented. The experimental prototype is shown in Figure 13. The control algorithm of the rectifier-chopper and the auxiliary compensator is realised by DSP(TMS320F28335).

3.2.1 | Cost assessment

This section will qualitatively assess and compare the cost of the traditional rectifier-chopper and the proposed rectifier-chopper

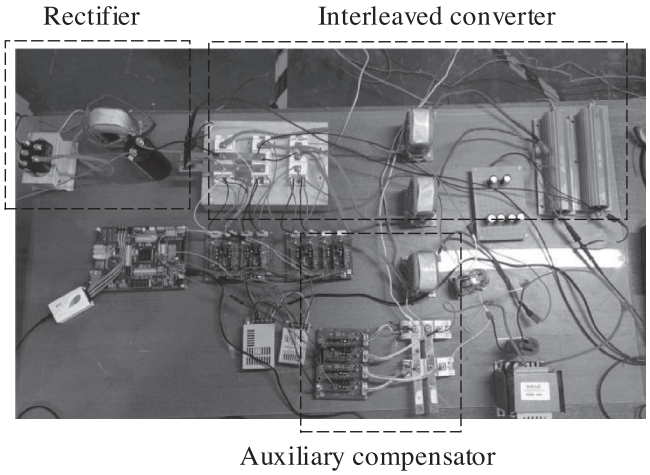

FIGURE 13 Experimental prototype.

with the auxiliary compensator. It is well known that the highest cost of a high-current converter is the filter inductor. With the proposed auxiliary compensator, the filter inductance can be reduced several times, which results in a significant reduction in the cost of the converter. Although the auxiliary compensator causes the use of additional devices, the auxiliary compensator is characterised by low power because only the ripple current flows through it. This means that the devices used in the auxiliary compensators are reasonably inexpensive. For example, low-power MOSFETs can be used for switching devices and inductors with low current ratings can be used. In total, the auxiliary compensator imposes a minimal cost burden on the converter but, on the contrary, significantly reduces the cost of the filter inductor of the converter.

3.2.2 | Experimental verification of output ripple

In this experiment, the rectifier-chopper consists of a three-phase diode rectifier bridge and a two-phase interleaved buck converter. There is a voltage fluctuation whose frequency and peak-to-peak value are 300 Hz and 4V, respectively, at the output side of the rectifier bridge, as shown in Figure 14.

The output current i_P of the traditional rectifier-chopper contains a low-frequency ripple and a medium-frequency switching ripple. Their waveforms can be observed from different time scales, as shown in Figure 15. The low-frequency ripple Δi_L is at the same frequency as the voltage U_d, fluctuating at a peak-to-peak value of about 1.4A, as shown in Figure 15a. In addition, the medium-frequency switching ripple Δi_S is superimposed on i_P, as shown in Figure 15b. Affected by the low switching frequency, the amplitude of Δi_S is up to about 1.8A. With the auxiliary compensator, a flow path is provided for the output ripple. The alternating current Δi_C in the auxiliary compensator is complementary to Δi_L and Δi_S. Therefore, the output ripple can be eliminated by the auxiliary compensator. It can be observed that The ripple of the output current is reduced to 0.1A, a reduction of 30 times compared to the current i_P.

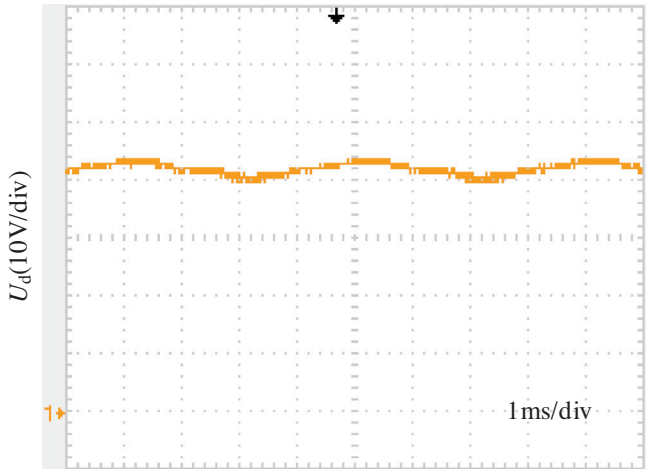

FIGURE 14 Voltage waveform at the output side of the rectifier bridge.

TABLE 3 Efficiency and losses of rectifier-choppers.

	i_O/A	P_t/W	P_n/W	P_a/W	η_t/%	η_n/%
Calcu-lation results	3	8.29	8.36	0.52	87.2	87.1
	6	12.84	11.34	0.52	89.3	90.6
	9	20.07	15.63	0.52	88.9	91.4
Experi-mental results	3	9.31	8.92	0.62	84.5	85.4
	6	16.81	13.44	0.60	86.0	88.8
	9	28.94	20.63	0.60	83.9	88.5

To validate the effectiveness of the proposed rectifier-chopper with the auxiliary compensator, a comparative experiment is being conducted. The experiment aims to evaluate and compare the output current ripple of the rectifier-chopper proposed in this paper with that of the rectifier-chopper with stacked interleaved buck proposed in the literature [5]. The experimental result demonstrates that although both rectifier-choppers effectively eliminate switching ripple, the rectifier-chopper with stacked interleaved buck fails to suppress the output low-frequency ripple, resulting in a substantial amplitude of roughly 1.4A, as shown in Figure 16. Conversely, the proposed rectifier-chopper with the auxiliary compensator successfully suppresses the low-frequency ripple, resulting in an output current ripple of approximately 0.1A. These comparison results prove the superior performance of the proposed rectifier-chopper with the auxiliary compensator.

3.2.3 | Loss assessment

Based on the above loss formulae and device datasheet, the theoretical losses of rectifier-choppers are calculated and verified by experimental results, as shown in Table 3. Calculation and experimental results include the loss P_t and efficiency η_t of the traditional rectifier-chopper, the loss P_n and efficiency η_n of the proposed rectifier-chopper with an auxiliary compensator,

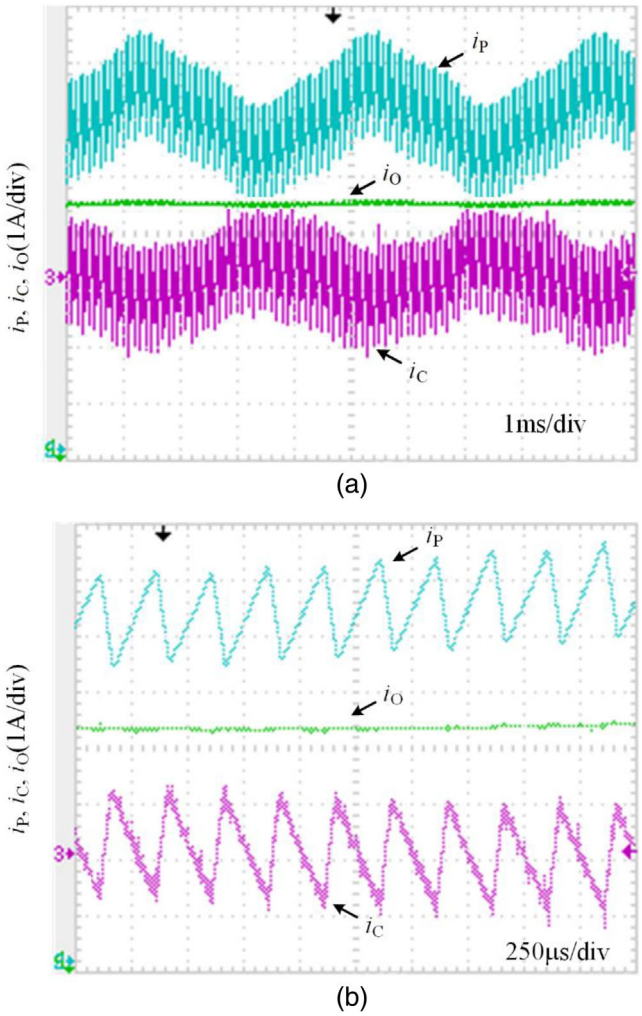

FIGURE 15 Output current waveforms of the experimental prototype. (a) Large time scale; (b) small time scale.

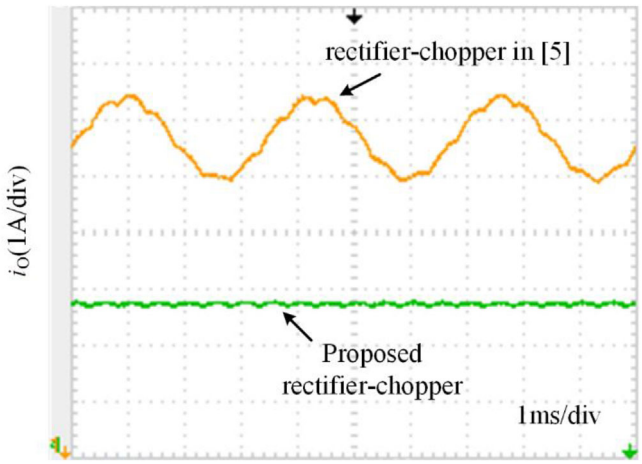

FIGURE 16 Output ripple comparison between the proposed rectifier-chopper and the rectifier-chopper in [5].

and the loss P_a of the auxiliary compensator. The experiment keeps the output voltage constant and adjusts the output current to change the power level. Theoretical calculation results show that the higher the output current, the more significant the efficiency improvement due to the auxiliary compensator. Note that the loss in the auxiliary compensator is not affected by the output current, as only a constant output AC ripple current flows through it. As the output current increases, the proposed rectifier-chopper with the auxiliary compensator improves efficiency by up to 4.6% over the traditional rectifier-chopper in the experiment.

The experimental results can effectively verify the theoretical calculation results. The experimental results show that the actual losses are higher than the theoretical calculations. This may be because some of the relatively small loss parts are ignored in the theoretical calculations.

4 | CONCLUSION

This paper proposes an AC-DC rectifier-chopper with an auxiliary compensator for hydrogen production applications. The proposed rectifier-chopper can maximise efficiency while eliminating the current ripple, including low-frequency and medium-frequency switching ripple. The application of the auxiliary compensator establishes a distinct path for these two types of ripples at the output of the rectifier-chopper, thereby averting any resulting ripple from reaching the load. Theoretically, the topology, control strategy, ripple elimination principle and loss calculation of the proposed rectifier-chopper were analysed in this paper. The effectiveness of the theory is verified by simulation and experimental results. The simulation and the experimental results can be concluded as follows: 1) without increasing the filter and switching frequency, the auxiliary compensator can eliminate the output current ripple of the rectifier-chopper; 2) the auxiliary compensator is characterised by low voltage and power level and therefore lead to little cost and loss; 3) the proposed rectifier-chopper with the auxiliary compensator improves efficiency by up to 4.6% over the traditional rectifier-chopper, and the higher the power level, the more significant the efficiency improvement.

AUTHOR CONTRIBUTIONS

Li Zhang: Conceptualization; validation; writing—original draft; writing—review & editing. **Minxiao Han**: Methodology; project administration. **Weiqi Bao**: Software. **Yijiang Dong**: Data curation; resources. **Yiwen Fan**: Formal analysis. **Haijun Liu**: Funding acquisition; investigation.

ACKNOWLEDGEMENTS

This work was supported by the National Key Research and Development Plan of China (No. 2020YFB1506800).

CONFLICT OF INTEREST STATEMENT

We declare that we do not have any commercial or associative interest that represents a conflict of interest in connection with the work submitted.

DATA AVAILABILITY STATEMENT

The data that support the findings of this study are available from the corresponding author upon reasonable request.

ORCID

Li Zhang https://orcid.org/0000-0002-1062-1148
Yiwen Fan https://orcid.org/0000-0003-3839-8715

REFERENCES

1. Bagherian, A., Nouri, T., Shaneh, M., et al.: An interleaved Zvs ultra-large gain converter for sustainable energy systems applications. IET Power Electron. 14(9), 1606–1621 (2021)
2. Hasanpour, S., Siwakoti, Y., Blaabjerg, F.: New single-switch quadratic boost Dc/Dc converter with low voltage stress for renewable energy applications. IET Power Electron. 13(19), 4592–4600 (2020)
3. Nirmal, S., Sivarajan, K.N., Jasmin, E.A.: Phase shift control and controller area network assisted proportional resonant control for grid integration of single phase voltage source inverters. IET Power Electron. 14(7), 1371–1383 (2021)
4. Sun, Y.S., Zhao, Z.X., Yang, M., et al.: Overview of energy storage in renewable energy power fluctuation mitigation. CSEE J. Power Energy Syst. 6(1), 160–173 (2020)
5. Guilbert, D., Vitale, G.: Improved hydrogen-production-based power management control of a wind turbine conversion system coupled with multistack proton exchange membrane electrolyzers. Energies 13(5), 1–18 (2020)
6. Mehrenjani, J.R., Gharehghani, A., Nasrabadi, A.M., et al.: Design, modeling and optimization of a renewable-based system for power generation and hydrogen production. Int. J. Hydrogen Energ. 47(31), 14225–14242 (2022)
7. Nguyen, B.L.H., Panwar, M., Hovsapian, R., et al.: Power converter topologies for electrolyzer applications to enable electric grid services. In: IECON 2021—47th Annual Conference of the IEEE Industrial Electronics Society. IEEE, Piscataway (2021)
8. Yodwong, B., Guilbert, D., Phattanasak, M., et al.: AC-DC converters for electrolyzer applications: State of the art and future challenges. Electronics 9(6), 1–31 (2020)
9. Guilbert, D., Sorbera, D., Vitale, G.: A stacked interleaved DC-DC buck converter for proton exchange membrane electrolyzer applications: Design and experimental validation. Int. J. Hydrogen Energ. 45(1), 64–79 (2020)
10. Buitendach, H.P.C., Gouws, R., Martinson, C.A., et al.: Effect of a ripple current on the efficiency of a pem electrolyser. Results Engr. 10, 1–13 (2021)
11. Rodriguez, J.R., Pontt, J., Silva, C., et al.: Large current rectifiers: state of the art and future trends. IEEE Trans. Ind. Electron. 52(3), 738–746 (2005)
12. Solanki, J., Frohleke, N., Bocker, J., et al.: High-current variable-voltage rectifiers: State of the art topologies. IET Power Electron. 8(6), 1068–1080 (2015)
13. Wang, C., Liu, X.N., Fei, W., et al.: Preliminary design of power supply for water-cooled resistive magnet based on three-level buck converters. IEEE Trans. Appl. Supercond. 1-4, 30(4) (2020)
14. Chen, Z., Luo, Y.P.: Low-harmonic-input three-phase rectifier with passive auxiliary circuit: Comparison and design consideration. IEEE Trans. Ind. Electron. 58(6), 2265–2273 (2011)
15. Marinescu, R.F., Nicolae, P.M., Firiuca, D.G., et al.: Aspects of power quality improvement in a driving system using an active filter. In: 2017 International Conference on Modern Power Systems (MPS). IEEE, Piscataway (2017)
16. Poonnoy, N., Mungporn, P., Thounthong, P., et al.: Differential flatness based control of 3-Phase AC/DC converter. European Conference on Electrical Engineering and Computer Science. IEEE, Piscataway (2017)
17. Naseri, F., Samet, H.: A comparison study of high power igbt-based and thyristor-based AC to DC converters in medium power DC arc furnace

plants. In: 2015 9th International Conference on Compatibility and Power Electronics (CPE), pp 14–19 (2015)
18. Sayed, K., Gronfula, M.G., Ziedan, H.A.: Novel soft-switching integrated boost DC-DC converter for Pv power system. Energies 13(3), 1–17 (2020)
19. Solanki, J., Frohleke, N, Bocker, J.: Implementation of Hybrid Filter for 12-pulse thyristor rectifier supplying high-current variable-voltage DC load. IET Electr. Power Appl. 62(8), 4691–4701 (2015)
20. Li, Y., Luo, L., Rehtanz, C., et al.: An industrial DC power supply system based on an inductive filtering method. IEEE Trans. Ind. Electron. 59(2), 714–722 (2012)
21. Unruh, R., Schafmeister, F., Bocker, J., et al.: Evaluation of Mmcs for high-power low-voltage DC-applications in combination with the module Llc-design. In: 22nd European Conference on Power Electronics and Applications Paderborn. IEEE, Piscataway (2020)
22. Yodwong, B., Guilbert, D., Kaewmanee, W., et al.: Energy efficiency based control strategy of a three-level interleaved DC-DC buck converter supplying a proton exchange membrane electrolyzer. Electron. 8(9), 1–19 (2019)

How to cite this article: Zhang, L., Han, M., Bao, W., Dong, Y., Fan, Y., Liu, H.: Low-Ripple high-efficiency AC-DC rectifier with auxiliary compensator for hydrogen production. IET Power Electron. 16, 2091–2102 (2023). https://doi.org/10.1049/pel2.12530